


## ORIGINAL RESEARCH

# Performance evaluation of PUC7-based multifunction single-phase solar active filter in real outdoor environments: Experimental insights

Soufiane Khettab<sup>1</sup> | Aissa Kheldoun<sup>2</sup> | Rafik Bradai<sup>3</sup> | Adel Oubelaid<sup>4</sup> | Sandeep Kumar<sup>5</sup> | Nima Khosravi<sup>6,7</sup> 

<sup>1</sup>SET Laboratory, Faculty of Technology, Electronics Department, Blida 1 University, Blida, Algeria

<sup>2</sup>Laboratory of Signals and Systems, Institute of Electrical and Electronic Engineering, University M'hamed Bougara, Boumerdes, Algeria

<sup>3</sup>LATSI, Faculty of Technology, Electronics Department, Blida 1 University, Blida, Algeria

<sup>4</sup>Faculté de Technologie, Laboratoire de Technologie Industrielle et de l'Information, Université de Bejaia, Bejaia, Algeria

<sup>5</sup>Chitkara Centre for Research and Development, Chitkara University, Himachal Pradesh, India

<sup>6</sup>Department of Electrical and Instrumentation Engineering, R&D Management of NPC, Tehran, Iran

<sup>7</sup>Centre of Research Impact and Outcome, Chitkara University Institute of Engineering and Technology, Chitkara University, Rajpura, Punjab, India

**Correspondence**

Nima Khosravi, Department of Electrical and Instrumentation Engineering, R&D Management of NPC, Tehran, Iran.  
Email: [nimakhosravi64@gmail.com](mailto:nimakhosravi64@gmail.com)

**Abstract**

This paper presents a novel architecture to enhance the performance of grid-connected photovoltaic (PV) systems through the introduction of several key novelties. Firstly, a packed U-cell seven-level (PUC7)-based single-phase solar active filter is implemented, offering a comprehensive solution for harmonics mitigation, reactive power compensation, and efficient power extraction from the PV source, while facilitating the injection of real power into the grid. Secondly, the p-q power injection algorithm is modified to accommodate the extraction of solar power from the PV generator to the grid, simultaneously addressing the need for harmonic current injection to improve power quality. This modification ensures dynamic performance by extracting reference current with harmonic content and solar power information, thereby enhancing the system's overall efficiency. Lastly, the proposed architecture undergoes real outdoor testing, validating its performance in various key aspects including maximum power tracking, reduction of total harmonic distortion in comparison with previous work, operation at unity power factor, and testing the effective operation of the multifunction feature. These contributions collectively demonstrate the effectiveness of the proposed system in enhancing power injection quality and reactive power compensation under real outdoor conditions of PV systems connected to the grid.

## 1 | INTRODUCTION

Recently, there has been a substantial worldwide increase in the use of renewable energies [1, 2]. This extensive adoption is motivated by the necessity to reduce the overdependence on traditional energy sources, which are known to contribute to environmental pollution. Utility companies are requesting more solar energy systems to be installed than ever before, driven by advancements in renewable energy sources [3–5]. As a result, there has been a growing focus on PV systems connected to the grid and the power conversion topologies they use.

Voltage source inverters (VSIs) are essential to improving the quality of the injected power in the grid-tied process [6–8], achieving this by removing current harmonics and adjusting the grid's reactive power at the point of common coupling (PCC) [9, 10]. Reactive power is required by local linear AC loads or non-linear loads, while harmonics are generated by the connection of power electronics-interfaced loads and generators. Reactive power consumption in electric power systems alters its operation from both economic and technical points of view while the presence of harmonics is strongly undesirable. They contribute in overheating the key equipment of power systems:

This is an open access article under the terms of the [Creative Commons Attribution-NonCommercial](https://creativecommons.org/licenses/by-nc/4.0/) License, which permits use, distribution and reproduction in any medium, provided the original work is properly cited and is not used for commercial purposes.

© 2024 The Author(s). *IET Renewable Power Generation* published by John Wiley & Sons Ltd on behalf of The Institution of Engineering and Technology.

transformers and generators. Classical passive filters are no longer appropriate solutions because of their limitations such as bulkiness, possible resonance, and load-dependent effectiveness. To this, active filters appear to be the appropriate solution as they can ensure both reactive power compensation and harmonic mitigation. Furthermore, compared to passive filters, they provide a fine response in spite of changing loads and harmonic variations. However, they are expensive and not affordable for every non-linear load. Nowadays, researchers are attracted by the tremendous growth in PV energy installation which are connected to the grid utility through inverters. Therefore, the economic solution is to take advantage of any grid-tied PV system and use it for other purposes such as active filtering and reactive power compensation. Several studies have proposed such topology being based on the two-level VSIs to act as multifunction active filter [11–14]. These topologies have shown a good performance for eliminating current harmonics and compensating for reactive power. However, two-level VSIs have two main drawbacks which are (1) high harmonic content of its output voltage and (2) high switching losses.

Moreover, using a multilevel inverter as an interface between the PV array and the PCC in the grid can enhance power quality (PQ) by generating multi-level voltages that approximate the desired shape. The multilevel inverter outperforms the traditional two-level inverter in producing AC voltages and currents with reduced harmonic distortion. Many recent papers have focused on multilevel inverter (MLI) topologies, including the flying capacitors inverter, neutral-point-clamped inverter [15], cascaded H-bridge inverter [16], and packed 'U' cells (PUCs) inverter [17]. PUC is the most commonly used topology in single-phase applications due to its superior economy compared to other topologies [18].

PUC7 stands out as the superior choice compared to both PUC5 and classical inverters due to its higher power conversion efficiency, improved power density and size, enhanced reliability, and durability. These advantages make PUC7 the preferred option for various applications, ranging from renewable energy systems to electric vehicles and industrial automation. PUC7 inverter has been suggested for this application due to its low component count and ability to generate seven output voltage levels [19]. Several control strategies have been proposed for grid-tied PUC inverters, such as traditional PI controllers using modulation techniques [20, 21]. However, there are some drawbacks to this approach, including hard implementation, complexity of the PWM modulator, and challenges in balancing capacitor voltages. Multi-objective MPC techniques have recently been created for PUC inverters [22]. Predictive control relies on a system model to anticipate the future behaviour of controlled variables, guiding optimal actuation based on predefined criteria. Hysteresis-based predictive control: This method modifies actuation in response to anticipated behaviour in an effort to keep variables within predetermined hysteresis boundaries. The approach of trajectory-based control involves directing the system to closely follow a predetermined route in order to force variables to follow it. Deadbeat management, by taking decisive action to decrease error and aim for instantaneous convergence, this approach aims to reach zero error in the

next sampling moment. MPC is a method of improving actuation by taking future predictions into account. This minimizes the given cost function. These methods provide many methodologies to accomplish control goals, each adapted to particular system specifications and performance standards. The reasons we chose MPC for our control application were its adaptability, capacity to follow trajectories, optimal control performance, and capacity to manage intricate restrictions.

The MPC technique is an easy-to-use and efficient way to manage MLIs. It has received a great deal of research in power converter control [23, 24]. By employing this technique, fewer PI controllers are needed, and a modulation step is not required. Furthermore, DC-link capacitor voltage balancing is a simple addition to the control target that results in a considerably cleaner converter output. The MPC method is based on estimating how controlled variables will behave in the future for each switching scenario and comparing the results to references using a cost function to get the best possible state. In addition, the MPC offers several intriguing features including precise tracking, quick dynamic response, and the capacity to include restrictions and non-linearities in controller design [25].

Many configurations of double-stage solar active filters are proposed in the literature. Each one has its features and differs from the others with respect to the type of inverter, the MPPT algorithm, the number of sensors, the control strategy, the validation method, or the achieved results etc. Each configuration can be evaluated as better than the others from one aspect or/and many aspects particularly the performance indices such as THD and power factor. In [26] and [27], the authors employed an H-bridge inverter with an LCL filter for PV power integration into the grid. However, these configurations did not consider the active filtering function and validated their proposals using PV emulators. However, authors in [28] employed an H-bridge inverter with an L-filter as the active power filter, yet encountered higher THD levels, and notably, a classical inverter was utilized. The authors in [29] opted for a modified PUC5 inverter with an L filter for active power injection. However, they validated their proposal using hardware-in-the-loop (HIL) simulations.

This paper presents the development and the outdoor implementation of a single-phase grid-tied PV system using a PUC7 multilevel inverter. To control the single-phase active filter while injecting the solar power into the grid, a modified MPC technique has been employed. This strategy aims to offset the impact of a contaminated load with a low power factor, improve reactive power control, eliminate harmonic currents content at the PCC, and inject real power generated by a PV array with low THD. Furthermore, during periods when PV power is unavailable, such as at night, the proposed architecture continues to provide services such as reactive power compensation and harmonic mitigation, enhancing the quality of power drawn from the grid. In order to offer high power factor correction, limit switching frequency, reduce computational, and guarantee DC-link capacitor voltage balancing, the suggested MPC method is used. Detailed simulations in the MATLAB/Simulink environment are used to verify the performance of this setup, and an experimental validation utilizing a real-time CU-SLRT Std.

(DS1104 Equivalent interface and features) is conducted without the use of temperature and irradiance sensors. This work's main contributions are summed up as follows:

- A new architecture of multifunction solar active power using double-stage, single-phase PUC7 inverter is proposed.
- A newly developed MPC algorithm is used for PUC7 inverter to ensure the power injection and voltage balance of the source and the capacitor.
- A real-time CU-SLRT Standard (DS1104 Equivalent interface+ features) is used to implement and validate the suggested control method while an  $I$ - $V$  tracer is designed to support the validation process.
- The efficiency of the multifunctional solar active filter architecture that has been suggested is validated under real outdoor conditions. Neither PV emulators nor weather sensors (temperature and irradiance) are used for the implementation.

The remainder of the paper is divided into the following sections: the system components as well as their mathematical models are outlined in Section 2. The latter is broken down into subsections where the PV array modelling is presented in Section 2.1, while the DC/DC boost converter and the DC-link regulator are controlled using the maximum power point tracking (MPPT) algorithm, which is briefly explained in Section 2.2. Section 2.3 introduces the PUC7 topology configuration, and Section 2.4 introduces the p-q modified power injection. Section 2.5 presents the suggested MPC method for the PUC7 inverter in grid-tied and active power filter (APF) applications. Section 3 presents the simulation results. In order to verify the excellent performance of the suggested system architecture, experimental findings with implementation utilizing a real-time CU-SLRT standard (DS1104-like interface) are described in Section 4. Finally, concluding remarks are drawn in Section 5.

## 2 | SYSTEM CONFIGURATION

The proposed configuration of the double-stage, single-phase PUC7 inverter, along with the proposed MPC controller and its corresponding control scheme, is illustrated in Figure 1. The system that is being studied consists of an AC source, a non-linear load that is connected in series, and the PUC7 inverter that is connected in parallel to the grid via a line inductor ( $L_f$ ) at the PCC. The PV system is connected to the PUC7 inverter's single DC-link capacitor by means of a boost converter, which has the ability to raise the voltage of the PV array to a high DC-link voltage. The main objectives of this specific configuration are the efficient integration of generated PV power into the electrical grid while ensuring high-quality grid current. Furthermore, this setup aims to address reactive power compensation and alleviate harmonic components induced by non-linear loads at the PCC.

### 2.1 | PV array modelling

Through the photovoltaic effect, solar radiation is directly converted into DC electric power using a photovoltaic cell. Following its operation, the electric circuit that is capable to simulate the behaviour of PV cell conversion consists of a DC current source connected in parallel with a diode as depicted by a dashed line in Figure 2a. Upon adding series and shunt resistance, the previous model is improved to account for the PV cell losses and leakage current in the PV junction. This model (Figure 2a) is widely adopted to model the behaviour of a real PV module [30–32]. Real-life applications of PV involve the connection of more than one module in series or in parallel. This PV array consists of  $N_{par}$  parallel strings with  $N_{ser}$  series-connected modules.

The output voltage is related to the PV array's output current by:

$$I_{PV} = N_{par} \cdot I_{pb} - N_{par} I_D - \frac{V_{PV} + I_{PV} \frac{N_{ser}}{N_{par}} \cdot R_s}{\frac{N_{ser}}{N_{par}} \cdot R_p} \quad (1)$$

The photocurrent, denoted as  $I_{pb}$ , is a variable that is influenced by both irradiance and temperature, as stated in Equation (2).

$$I_{pb} = \frac{G}{G_{ref}} (I_{pb\_ref} + \alpha_{T\_ISC} (T - T_{ref})) \quad (2)$$

The current flowing via a diode, denoted as  $I_D$ , is determined by the well-known Shockley equation:

$$I_D = I_S \left( \exp \left[ \frac{V_{PV} + I_{PV} \frac{N_{ser}}{N_{par}} \cdot R_s}{\alpha \cdot V_{tb} \cdot N_{ser}} \right] - 1 \right) \quad (3)$$

where  $\alpha$  is the ideality factor of the diode and  $I_S$  is the reverse saturation current that is given as

$$I_S = \frac{I_{SC, ref} + \alpha_{T\_ISC} (T - T_{ref})}{\exp \left[ \frac{V_{oc, ref} + \alpha_{T\_Voc} (T - T_{ref})}{a \cdot V_{tb} \cdot N_{ser}} \right]} \quad (4)$$

In the following,  $V_{tb}$  is the thermal voltage of  $N_s$  series connected cells constituting one PV module. This voltage mainly depends on the PV cell temperature:

$$V_{tb} = \frac{N_s K}{q} \cdot T \quad (5)$$

One must distinguish  $N_s$ , the number of a module's series-connected cells, from  $N_{ser}$ , the number of series-connected modules in a photovoltaic array.

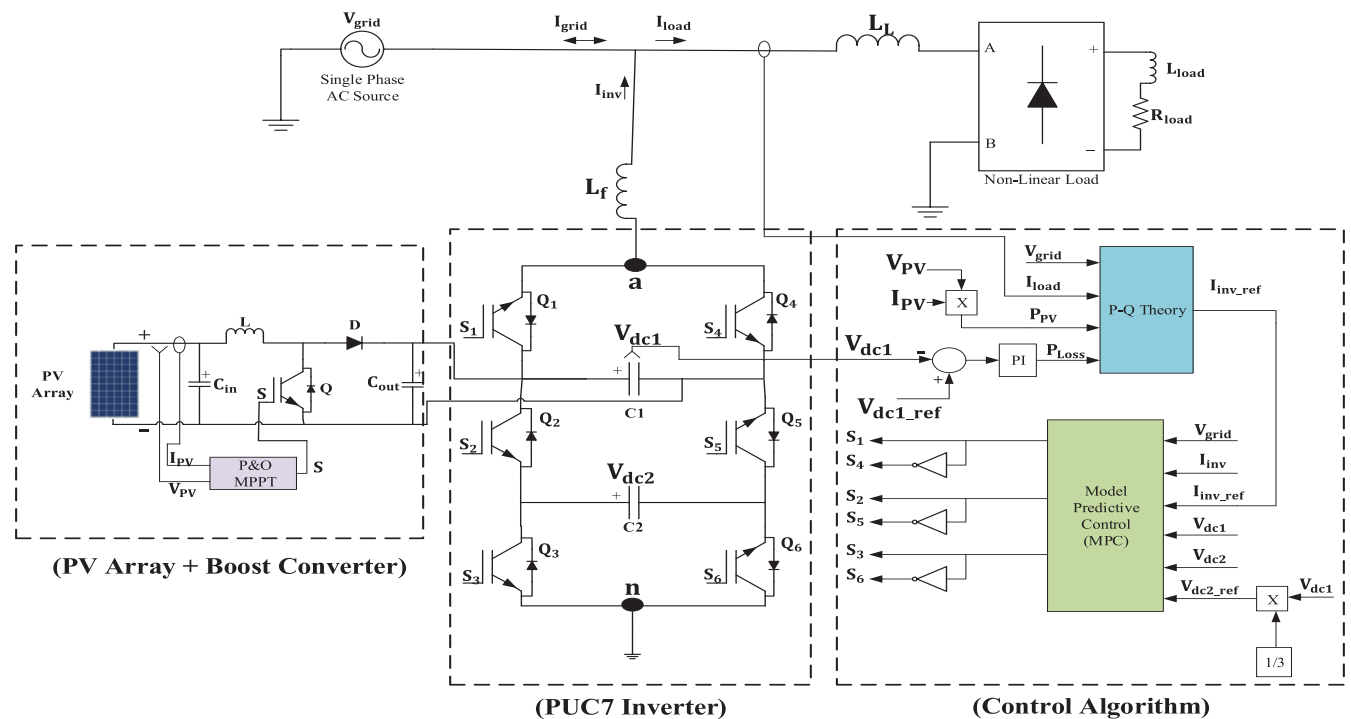


FIGURE 1 The proposed configuration of the double-stage, single-phase PUC7 inverter.

## 2.2 | MPPT controller

A method called maximum power point tracking (MPPT) can optimize a photovoltaic system's power generation under a variety of environmental circumstances. The MPP of the PV array is a unique point at which maximum power is obtained and this operating point corresponds to a given PV voltage and current obtained at a given environment and load conditions. One of the most commonly used MPPT algorithms is Perturb and Observe (P&O). It operates by altering the voltage or current of the PV array gradually and assessing the ensuing power.

The MPPT controller continues to adjust the voltage or current (by modifying the chopper's duty cycle) in the same direction if the power keeps increasing. When the power drops, the controller adjusts the control signal in the opposite direction. This process is repeated as many as needed to meet the condition stating that the variation of the power with respect to the change of the voltage or current is null. This point is known as the MPP of the ' $P$ - $V$ ' characteristic. These steps are summarized in the flowchart of P&O technique that is depicted in Figure 3. As can be noticed from the flowchart, the P&O algorithm is simple, easy to implement and therefore widely applicable [33, 34].

## 2.3 | PUC7 inverter

The configuration of the PUC converter is recent and it is based on the association of packed U cells where two switches and a capacitor constitute the cell [35]. The authors in [36] introduced

TABLE 1 PUC7 inverter state switching.

State switching ( $x$ )	$s_1$	$s_2$	$s_3$	$s_4$	$s_5$	$s_6$	$V_{an}$
State 1	1	0	0	0	1	1	$V_{dc1}$
State 2	1	0	1	0	1	0	$V_{dc1} - V_{dc2}$
State 3	1	1	0	0	0	1	$V_{dc2}$
State 4	1	1	1	0	0	0	0
State 5	0	0	0	1	1	1	0
State 6	0	0	1	1	1	0	$-V_{dc2}$
State 7	0	1	0	1	0	1	$V_{dc2} - V_{dc1}$
State 8	0	1	1	1	0	0	$-V_{dc1}$

the PUC inverter, which consists of six active switches, an isolated DC supply, and a DC capacitor that acts as a dependent DC source, as shown in Figure 1.

The PUC7 has the same number of components as other designs, but it has lower power losses and costs due to reduced switch count. Table 1 exhibits the output voltage levels, with switches  $S_1$ ,  $S_2$ , and  $S_3$  functioning in conjunction with switches  $S_4$ ,  $S_5$ , and  $S_6$ , respectively. It is important to note that each pair of switches, namely ( $S_1$ ,  $S_4$ ), ( $S_2$ ,  $S_5$ ), and ( $S_3$ ,  $S_6$ ), cannot be activated simultaneously.

The PUC inverter can produce seven levels of output voltage by using two capacitors. One-third of the DC bus voltage ( $V_{dc1}$ ) should be the capacitor's voltage ( $V_{dc2}$ ), so that the output voltage levels are  $0, \pm V_{dc2}, \pm 2 V_{dc2},$  and  $\pm 3 V_{dc2}$ . However, the primary constraint of the PUC7 inverter is that it cannot provide an output voltage greater than the DC bus voltage. The benefit of employing the PUC inverter lies in its capability to mitigate

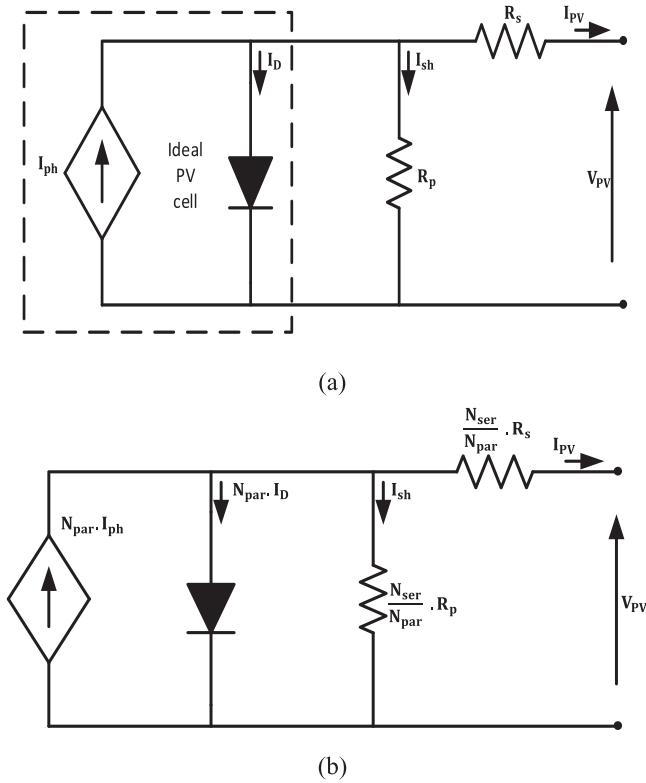


**FIGURE 2** The photovoltaic (PV) source's electrical modelling includes: (a) the PV array and (b) PV module.

load voltage harmonics by segmenting the DC bus voltage into multiple levels. This, in turn, diminishes the requirement for bulky filters at the inverter's output. The mathematical representation of the single-phase active power filter system utilizing the PUC7 inverter is depicted in the following equations:

$$\frac{dI_{inv}(t)}{dt} = -\frac{R_f}{L_f} I_{inv} + \frac{1}{L_f} (V_{an} - V_{grid}) \quad (6)$$

$$\frac{dV_{dc}(t)}{dt} = \frac{1}{C} I_{inv} \quad (7)$$

where  $V_{dc}$  is the voltage across the DC-link capacitor,  $I_{inv}$  and  $V_{grid}$  are the inverter's current and grid voltage, respectively.

The PUC7 inverter generates a voltage ( $V_{an}$ ) that is based on the states of the switches  $s_1$ ,  $s_2$  and  $s_3$ . To simplify the estimation of ( $V_{an}$ ), two variables,  $S_1$  and  $S_2$ , are defined based on the following equations:

$$S_1 = s_1 - s_2 \quad (8)$$

$$S_2 = s_2 - s_3 \quad (9)$$

Applying KVL to the PUC7 circuit shown in Figure 1 allows to derive the equation of the inverter's generated voltage, that is:

$$\begin{aligned} V_{an} &= V_{ab} + V_{bc} + V_{cn} \\ V_{an} &= (s_1 - 1) \cdot V_{dc1} + (1 - s_2) \cdot (V_{dc1} - V_{dc2}) + (1 - s_3) \cdot V_{dc2} \\ V_{an} &= (s_1 - s_2) \cdot V_{dc1} + (s_2 - s_3) \cdot V_{dc2} \end{aligned} \quad (10)$$

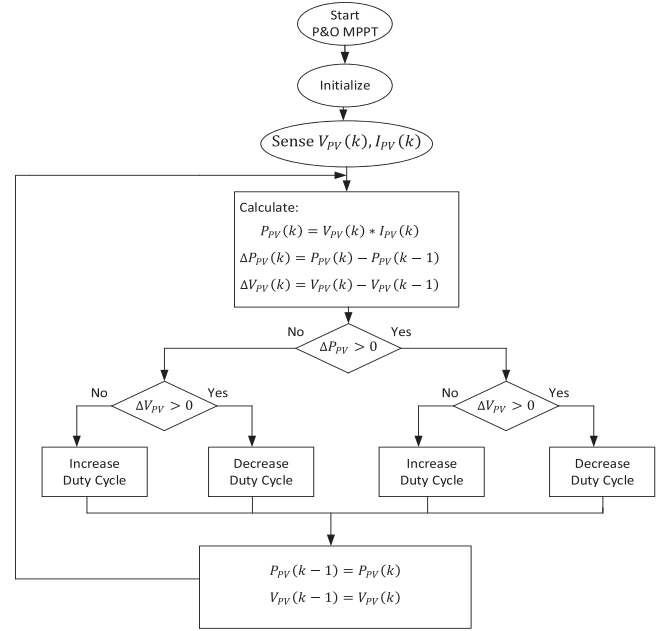


**FIGURE 3** The P&O method flowchart.

Upon substituting (8) and (9) in (10), one can find the simplified equation of  $V_{an}$

$$V_{an} = S_1 \cdot V_{dc1} + S_2 \cdot V_{dc2} \quad (11)$$

Moreover, the voltage across the capacitors may be described as follows in terms of their charging current:

$$\begin{aligned} V_{dc1} &= -S_1 \cdot \frac{1}{C_1} \int i_{inv} dt \\ V_{dc2} &= -S_2 \cdot \frac{1}{C_2} \int i_{inv} dt \end{aligned} \quad (12)$$

## 2.4 | Modified p-q theory for power injection

The theory of instantaneous reactive power, commonly referred to as the 'p-q' theory, stands out as one of the most effective approaches for obtaining instantaneous reference signals crucial for active power filtering. Originally designed for three-phase systems, encompassing both three- and four-wire configurations [37], the advantages of the multi-phase 'p-q' theory can now be expanded to single-phase systems through a recently proposed extension. Moreover, in scenarios involving unbalanced supply voltage and/or load conditions, the single-phase 'p-q' theory demonstrates the capability to generate a sinusoidal source current and efficiently manage multi-phase systems, surpassing the performance of the three-phase theory [38].

The core concept of the single-phase 'p-q' theory involves shifting the initial system voltage and current by  $\pi/2$  in either direction, creating a pseudo-two-phase system. This approach facilitates the expression of the entire system in  $\alpha$ - $\beta$  coordinates, where  $\alpha$ -axis values correspond to the initial source voltage and load current, and  $\beta$ -axis quantities result from the

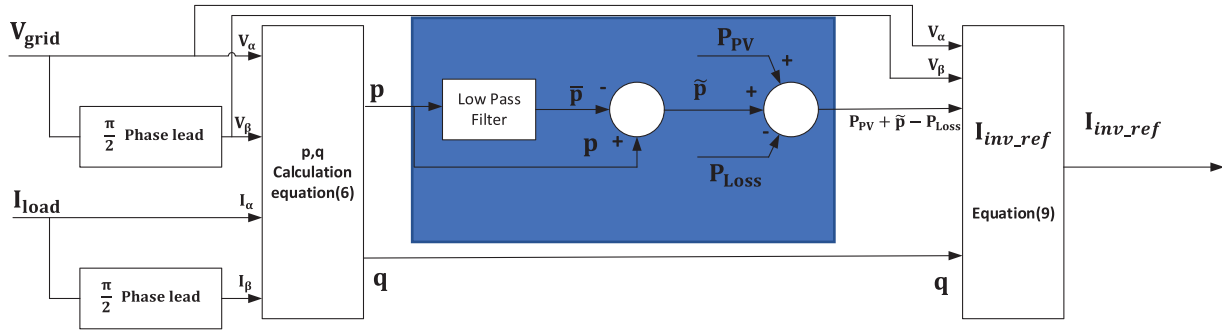


FIGURE 4 Modified 'p-q' power injection.

displacement of the source voltage and load current by  $\pi/2$ . The representation of single-phase source voltage involves a  $\pi/2$  forward shift in  $\alpha$ - $\beta$  coordinates.

$$\begin{bmatrix} V_{\alpha}(\omega t) \\ V_{\beta}(\omega t) \end{bmatrix} = \begin{bmatrix} V_{grid}(\omega t) \\ V_{grid}(\omega t + \frac{\pi}{2}) \end{bmatrix} \quad (13)$$

In a similar way, the load current representation in a coordinate system with a  $\pi/2$  forward shift.

$$\begin{bmatrix} I_{\alpha}(\omega t) \\ I_{\beta}(\omega t) \end{bmatrix} = \begin{bmatrix} I_{load}(\omega t) \\ I_{load}(\omega t + \frac{\pi}{2}) \end{bmatrix} \quad (14)$$

The power components 'p' and 'q' can be represented together since they are related to the same  $\alpha$ - $\beta$  voltages and currents.

$$\begin{bmatrix} p(\omega t) \\ q(\omega t) \end{bmatrix} = \begin{bmatrix} V_{\alpha}(\omega t) & V_{\beta}(\omega t) \\ -V_{\beta}(\omega t) & V_{\alpha}(\omega t) \end{bmatrix} \cdot \begin{bmatrix} I_{\alpha}(\omega t) \\ I_{\beta}(\omega t) \end{bmatrix} \quad (15)$$

The expressions for the  $p(\omega t)$  and  $q(\omega t)$  are:

$$p(\omega t) = \bar{p}(\omega t) + \tilde{p}(\omega t) \quad (16)$$

$$q(\omega t) = \bar{q}(\omega t) + \tilde{q}(\omega t) \quad (17)$$

The instantaneous fundamental active and reactive power is represented by the DC components  $\bar{p}(\omega t)$  and  $\bar{q}(\omega t)$ , while the harmonic power is represented by the AC components  $\tilde{p}(\omega t)$  and  $\tilde{q}(\omega t)$ . In the following, the AC component ( $\tilde{p}(\omega t)$ ) of active power and the overall reactive power ( $q(\omega t)$ ) are employed for computing the harmonic reference current.

To counterbalance voltage source inverter switching losses and maintain the desired DC-link voltage, the shunt active power filter draws a minimal amount of real power ( $P_{Loss}$ ) either from the single-phase AC source or an external power source. In addition to reducing harmonics, it will provide active power from the PV array connected via a boost converter to the inverter. To inject this power into the grid, we thus updated the PQ theory and included the PV power with the AC component ( $\tilde{p}(\omega t)$ ) of active power. Therefore, as seen in Figure 4, we need a

particular feedback signal to force the control circuit to include power and harmonics in its output. The reference compensating current can be obtained by this equation:

$$I_{inv\_ref} = \frac{((V_{\alpha} \times (P_{PV} + \tilde{p} - P_{Loss})) - V_{\beta} \times q)}{V_{\alpha}^2 + V_{\beta}^2} \quad (18)$$

## 2.5 | MPC procedure

MPC is a control technique that is more sophisticated and efficient than traditional PID control. It forecasts the future behaviour of the controlled variable using a mathematical model of the system under study. MPC is a powerful and successful technique for controlling power converters in general. The suggested MPC allows the PUC7 inverter to operate in both the active power filter and grid-connected PV system modes. The flowchart in Figure 5 illustrates the functionality of the suggested MPC.

For each of the eight switching states, the inverter current ( $I_{inv}$ ) measured values, grid voltage ( $V_{grid}$ ), and capacitor voltages ( $V_{dc1}$ ,  $V_{dc2}$ ) are used to calculate the anticipated values of the inverter current ( $I_{ref\_cal}$ ) and the capacitor voltage ( $V_{dc2\_cal}$ ). Next, the best switching state that matches its minimal value is chosen using a cost function ( $g$ ).

The switching pulses are created based on the suitable switching state picked up by the MPC from the switching table, and they provide the PUC7 inverter with the ideal switching state selected for the next sampling period. The variables that the suggested MPC must regulate are the capacitor voltage ( $V_{dc2}$ ) and the future inverter current ( $I_{inv}$ ). The cost function ( $g$ ) incorporates these control goals in the following function:

$$g = \lambda_1 (I_{ref\_cal}(k+1) - I_{inv\_ref}(k))^2 + \lambda_2 (V_{dc2\_cal}(k+1) - V_{dc2\_ref}(k))^2 \quad (19)$$

where the weighting factors are denoted by  $\lambda_1$  and  $\lambda_2$ . A branch and bound approach may be used to reduce the number of simulations needed to determine the appropriate value for the weighting factor. In our research, we adopt a uniform weighting factor, where both  $\lambda_1$  and  $\lambda_2$  are set to 1, instead of employing an optimization process to determine the appropriate

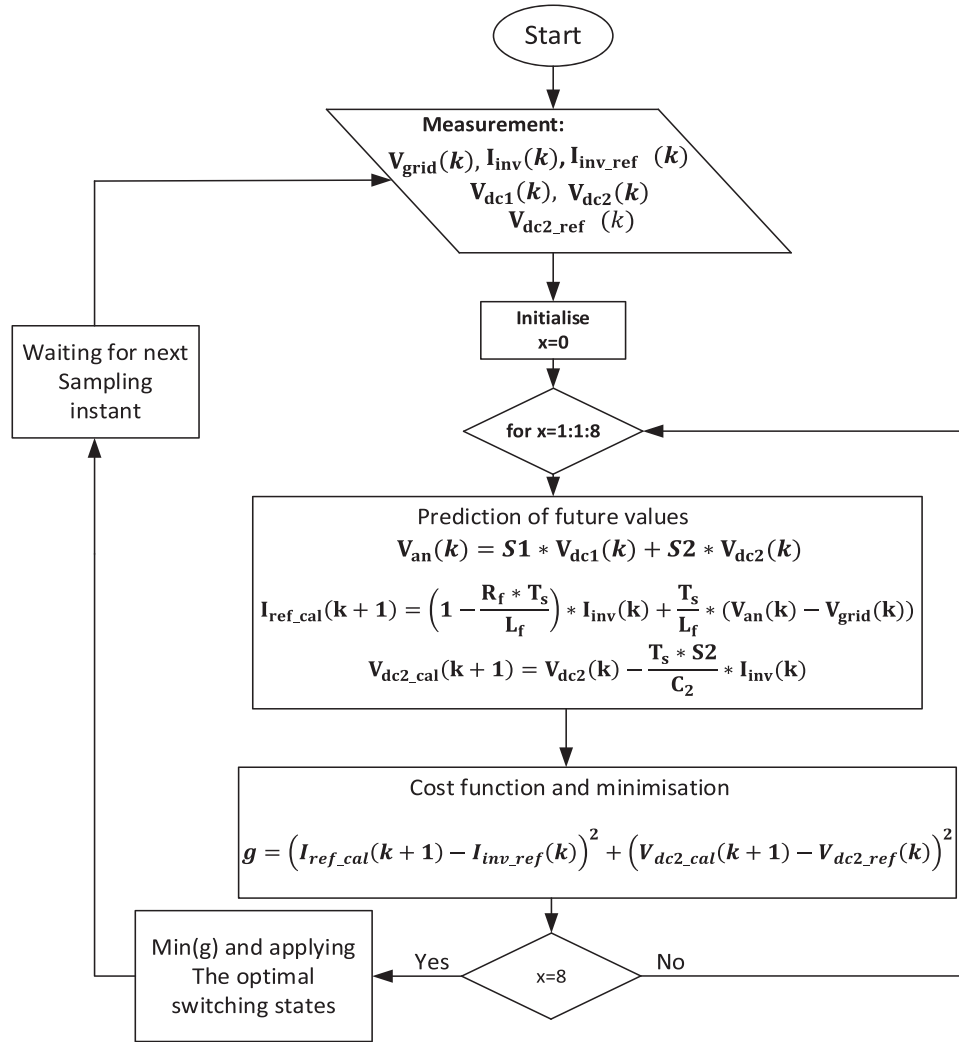


FIGURE 5 Model predictive control (MPC).

weighting factor. By adopting such a strategy, no tuning of parameters is required during the implementation of the controller.

The inverter current's reference and future values are provided by the variables  $I_{inv\_ref}(k)$  and  $I_{ref\_cal}(k+1)$ , respectively. Likewise, the reference and future values of the DC-link capacitor voltages are indicated by the variables  $V_{dc2\_ref}(k)$  and  $V_{dc2\_cal}(k+1)$ , respectively. These variables are essential for evaluating and regulating the inverter.

The derivative of the inverter current  $\frac{dI_{inv}(t)}{dt}$ , is replaced by a forward Euler approximation. In other words, the derivative of the current is reduced to the following formula:

$$\frac{dI_{inv}(t)}{dt} = \frac{I_{inv}(k+1) - I_{inv}(k)}{T_s} \quad (20)$$

Substituting Equation (20) in Equation (6) allows obtaining the equation to forecast the load current at the time  $(k+1) T_s$  in the future for each of the eight voltage vector values  $V_{an}(k)$  produced by the inverter.

This expression is given as:

$$I_{ref\_cal}(k+1) = \left(1 - \frac{R_f * T_s}{L_f}\right) * I_{inv}(k) + \frac{T_s}{L_f} * (V_{an}(k) - V_{grid}(k)) + \frac{T_s}{L_f} * (V_{an}(k) - V_{grid}(k)) \quad (21)$$

The derivative of the capacitor voltages may be calculated using the same estimate of the derivative as in the previous equation:

$$\frac{dV_{dc}(t)}{dt} = \frac{V_{dc}(k+1) - V_{dc}(k)}{T_s} \quad (22)$$

Combining Equation (7) and Equation (22), the capacitor voltage's discrete-time equation can be derived as follows:

$$V_{dc2\_cal}(k+1) = V_{dc2}(k) - \frac{T_s * S2}{C_2} * I_{inv}(k) \quad (23)$$

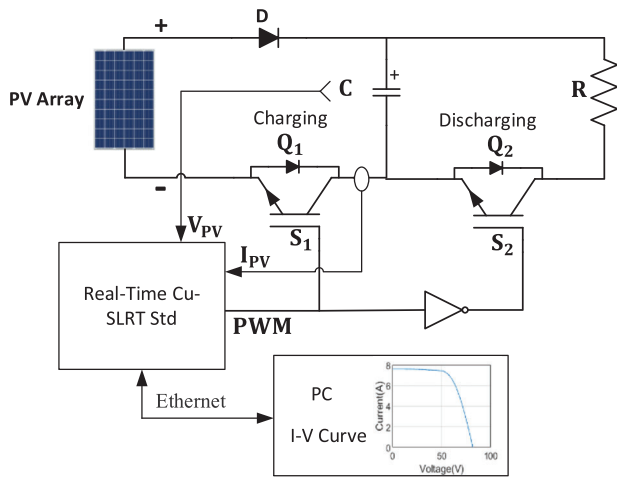


**FIGURE 6** The  $I$ - $V$  curve tracer using capacitor charging and discharging process.

### 3 | PV IDENTIFICATION AND SIMULATION RESULTS

#### 3.1 | PV array identification

Conducting simulation scenarios of PV system, whether it is islanded or grid-connected, requires the data of each component involved in the system depicted in Figure 1. The preceding section has outlined the modelling of each of these components. Some components are designed such, as the chopper, the inverter, and the filter, while others are computed, such as the parameters of the proposed controllers. However, the parameters of the PV array model, typically supplied by the manufacturer, are based on standard test conditions (STC) data. These parameters include open circuit voltage, short circuit current, maximum power, maximum power point voltage, and maximum power point current at STC. For simulation purposes, one needs the internal parameters of the PV array as well as those of the other PV system components. In the present study, an experimental setup is proposed to identify these parameters. Figure 6 shows the main components of the proposed setup. The PV array is connected to an RC circuit with two switches. The identification process is carried out in two steps: (1) measurement of  $I$ - $V$  curve, then (2) extraction of the PV array model's parameters. To obtain the  $I$ - $V$  curve, the capacitor is charged by turning on switch  $Q_1$  to the maximum voltage of the PV which is the open circuit voltage then discharged over the resistance to enable conducting the next measurement.

While the current drops from short-circuit current ( $I_{sc}$ ) to zero throughout the charging process, the capacitor's voltage rises from 0 to the PV array's open-circuit voltage ( $V_{oc}$ ). To get the PV current and voltage data, two sensors are used. The resulting  $I$ - $V$  may then be plotted, as seen in Figure 7a. The second step, aiming at extracting the PV parameters from the measured  $I$ - $V$  curve, is carried out by solving Equation (24):

$$RMSE = \frac{1}{n} \sum_{i=1}^N (I_{PV\_measured} - I_{PV})^2 \quad (24)$$

**TABLE 2** PV array identification results.

Value	7.6418	$6.1593 \cdot 10^{-8}$	1.1221	0.4273	146.389
Parameter	$I_{PV}$ (A)	$I_s$ (A)	$a$	$R_r$ ( $\Omega$ )	$R_p$ ( $\Omega$ )

where

- $I_{PV\_measured}$  is the measured PV current.
- $I_{PV}$  is the computed PV current.
- $N$  is the total number of measurements (samples).

It is evident from Equation (1) that in order to calculate the PV current, one must be aware of the model parameters. To do this, solving Equation (25) is converted to an optimisation process where a metaheuristic algorithm is employed, as detailed in [30, 38–41]. In fact, a modified African Vulture algorithm is selected for its good performance and then applied to minimize Equation (24). The acquired parameters of the PV array are displayed in Table 1. It has to be mentioned that besides the identification of the PV array parameters, the  $I$ - $V$  curve will be used to check the effectiveness of the proposed control system in both simulation and experimental validation.

$$RMSE = \frac{1}{n} \sum_{i=1}^N (I_{PV\_measured} - I_{PV})^2 \quad (25)$$

Upon substituting the parameters shown in Table 2 in the model of the PV array, Equations (1), (3) and (5), and solving them for the PV current, the  $I$ - $V$  curve of the PV array is obtained as shown in Figure 7b. Notice that the values of the voltage being used while solving Equations (1), (3) and (5) are those obtained from the experimental part.

#### 3.2 | Simulation results

To evaluate the performance of the suggested design, MATLAB/Simulink software, comprising every part of the PV system mentioned in Section 1, has been created. The simulation runs at a sampling frequency of 30 kHz, while the controller (MPC) operates at a sampling frequency of 20 kHz. Table 3 depicts the data of these components. Before performing both the experimentation and simulation test in order to assess the suggested PV system's efficacy, both experimental and simulated  $I$ - $V$  have been identified and used to derive the experimental and simulated  $P$ - $V$  curves, respectively, by multiplying the PV voltage by the PV current.

Figure 8 illustrates the measured and computed  $P$ - $V$  curves using extracted PV model parameters. They were obtained under the weather conditions when the PV array was identified. It has to be mentioned that, as stated in the objectives of this work, the proposed multifunction solar active filter is evaluated under real outdoor conditions without using both irradiance and temperature sensors. A contrast between the experimental and the simulated  $P$ - $V$  curves reveals that the real maximum power point, that is, 403.538 W corresponding to the



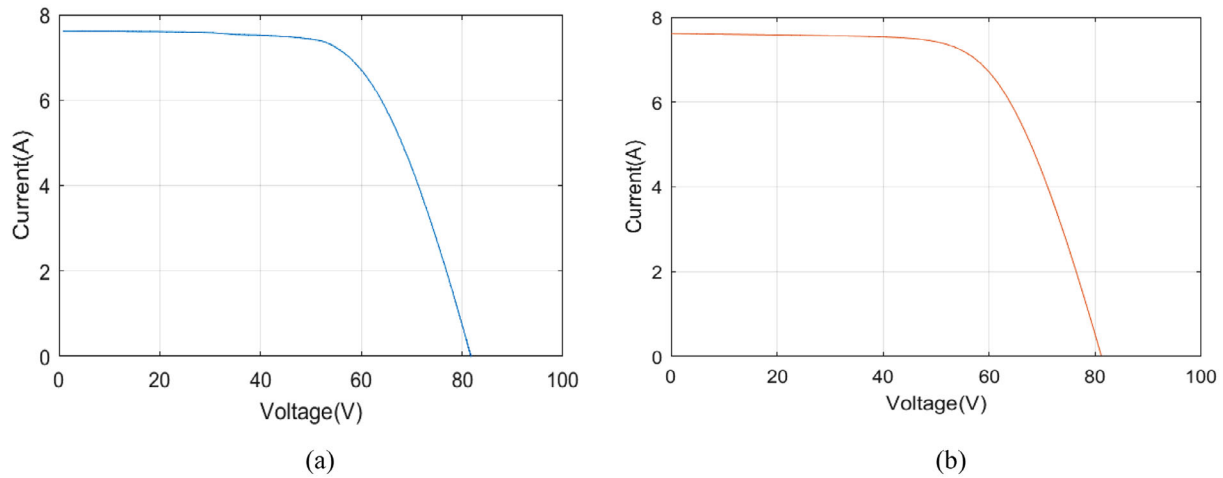


FIGURE 7  $I$ - $V$  properties of the PV array in use: (a) experimental curve, (b) simulated curve.

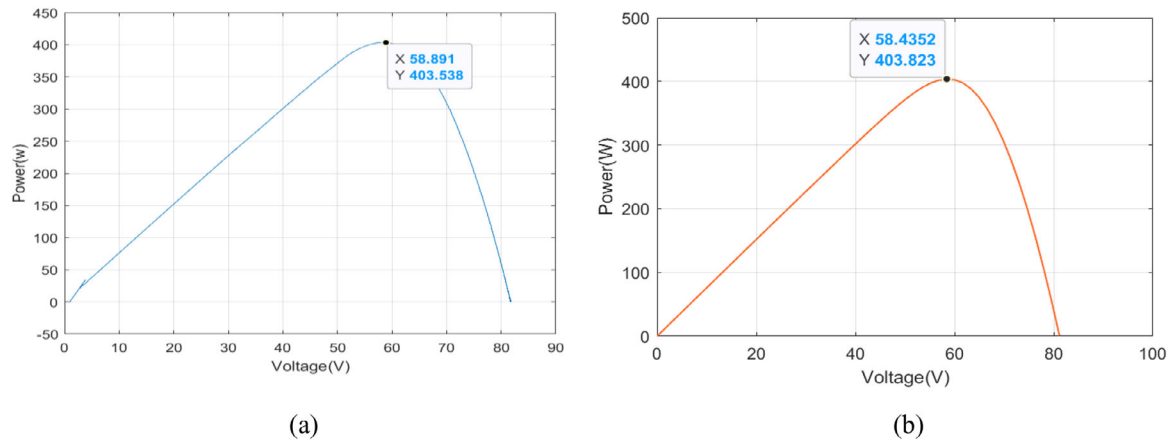


FIGURE 8  $P$ - $V$  properties of the PV array in use: (a) experimental curve, (b) simulated curve.

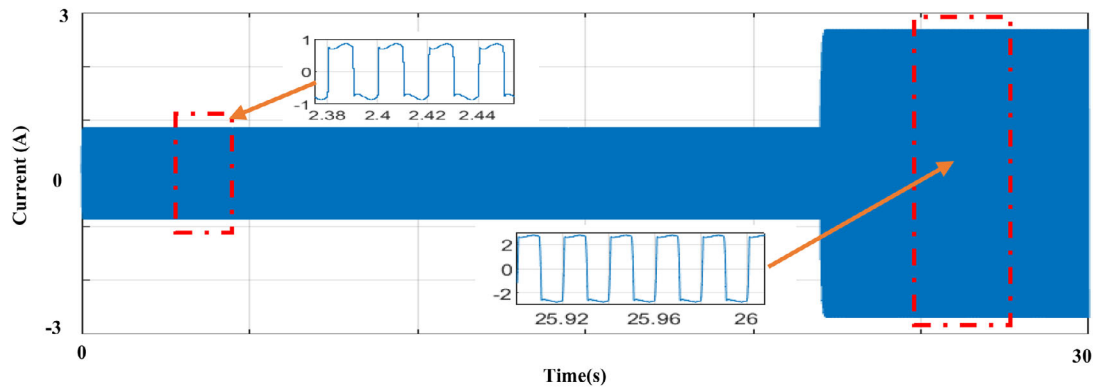
TABLE 3 PV system components specifications.

Grid	Grid voltage, $V_{grid}$ (RMS)	63 V
Non-linear load	Grid frequency, $F_s$	50 Hz
	AC-side rectifier inductor, $L_L$	3 mH
	DC side load: resistor, $R_{load}$	70 $\Omega$
	DC side load: inductor, $L_{load}$	0.7 H
Filter	Filter inductance, $L_f$	15 mH
PUC7 inverter	DC capacitor, $C_1 = C_2$	1500 $\mu$ F
	DC voltage reference	120 V
Boost converter	Input capacitor, $C_{in}$	47 $\mu$ F
	Output capacitor, $C_{out}$	390 $\mu$ F
	Inductance, $L$	5 mH
PV array (STC)	Maximum power ( $P_{max}$ )	600 W
	Open circuit voltage ( $V_{oc}$ )	90.5 V
	Short circuit current ( $I_{sc}$ )	8.49 A
	Maximum power voltage ( $V_{mp}$ )	74.6 V
	Maximum power current ( $I_{mp}$ )	8.04 A

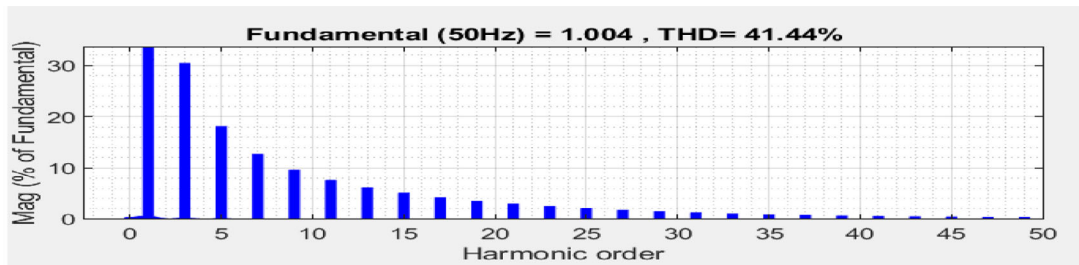
PV array voltage 58.891 V, is almost the same as that obtained by simulating the PV array using the extracted model parameters ( $P_{max} = 403.823$ ,  $V_{mp} = 58.4352$ V).

The proposed PV system architecture, under the irradiance and the temperature of the identification, has been simulated with different operating conditions. Therefore, the whole simulation time is broken down to three scenarios in order to evaluate the suggested control system's efficacy.

- The first scenario starts from 0 to 12 s and during which the PV array remains disconnected. The objective of this scenario is to check the filtering function of the proposed architecture.
- The second scenario begins from 12 s and ends at  $t = 22$  s. During this period, the inverter is linked to the PV array and therefore two distinct functions can be assessed; the direction of power from or to the grid utility, as well as the maximum power point tracking.
- Last scenario, starts at 22 s and ends at  $t = 30$  s. The non-linear load is varied in a way to increase its impedance and



(a)



(b)

**FIGURE 9** (a) Load current (b) Harmonic spectrum of the load current.

therefore the power to the grid is altered. During this period, the focus will be on the power balance assessment.

Figures 9a and 9b illustrate the current drawing by the non-linear load and its harmonic spectrum analysis respectively. The current looks constant during the first two scenarios. However, this current is drawn from the grid during the first scenario while from the PV during the second scenario. The control could ensure smooth switching between the two sources. Figure 9b shows the harmonic content of the load current that is evaluated by its THD of 41.44%. This level is far away from the one required by the standard of grid connection. The current's increase in the third scenario is due to the decrease of the resistance on the DC side; from  $70 \Omega$  to  $23 \Omega$ . Figure 10b depicts the variation of the inverter current and the reference current. The latter is generated by the modified 'p-q' power injection controller, while the MPC ensures the injection of this current into the PCC to mitigate these harmonics. It is clear that, during the two first periods, in spite of the switching between grid utility and the PV, the current being injected is the one that corresponds to the minimum THD and the requirement of the load in terms of power. As for the THD result, the grid current becomes sinusoidal and the THD remains less than 5% in all scenarios, according to the IEEE 519–2022 without making any changes to the non-linear load that keeps absorbing the distorted current. The worst THD is obtained during the power injection and it is evaluated as 2.63%. The voltage of the DC-link  $V_{dc}$  is kept at the reference value (120 V) as shown

in Figure 10c. Furthermore, a perfect voltage balance between the two capacitors  $V_{dc1}$  and  $V_{dc2}$  is achieved where the voltage across the second capacitor is kept constant and equal to one-third of the first cell capacitor voltage (40 V). This voltage constraint is required for the PUC7 inverter to deliver seven (7) level single-phase voltage. Figure 10d displays the PV's power, of the grid utility, and that of the load.

During the first scenario, there is no power coming from that PV and therefore the grid supplies the load. After the connection of the PV array, the control moved the power source from the grid to the photovoltaic array, sending any extra solar energy back to the grid (grid power is negative).

It is evident that the highest possible level of power harvesting is attained as the power drawn during the last two scenarios is matching with maximum power in the experimental PV shown in Figure 8a. Furthermore, during the last scenario, the increase in load has resulted in a decrease in the power being sent to the grid utility while power from the PV remains the same as long as there is no change in the weather conditions. In summary, this proposed control system has ensured the distribution of power between the grid, the PV source, and the non-linear load by giving priority to the PV and maintain the THD to its minimum level. As a result, as shown in Figure 10f, the suggested PUC7 inverter system shows very little leakage current. The aforementioned discovery highlights the appropriateness of the multilevel inverter (MLI) PUC7 architecture for single-phase PV applications involving low and medium-power conversion systems.

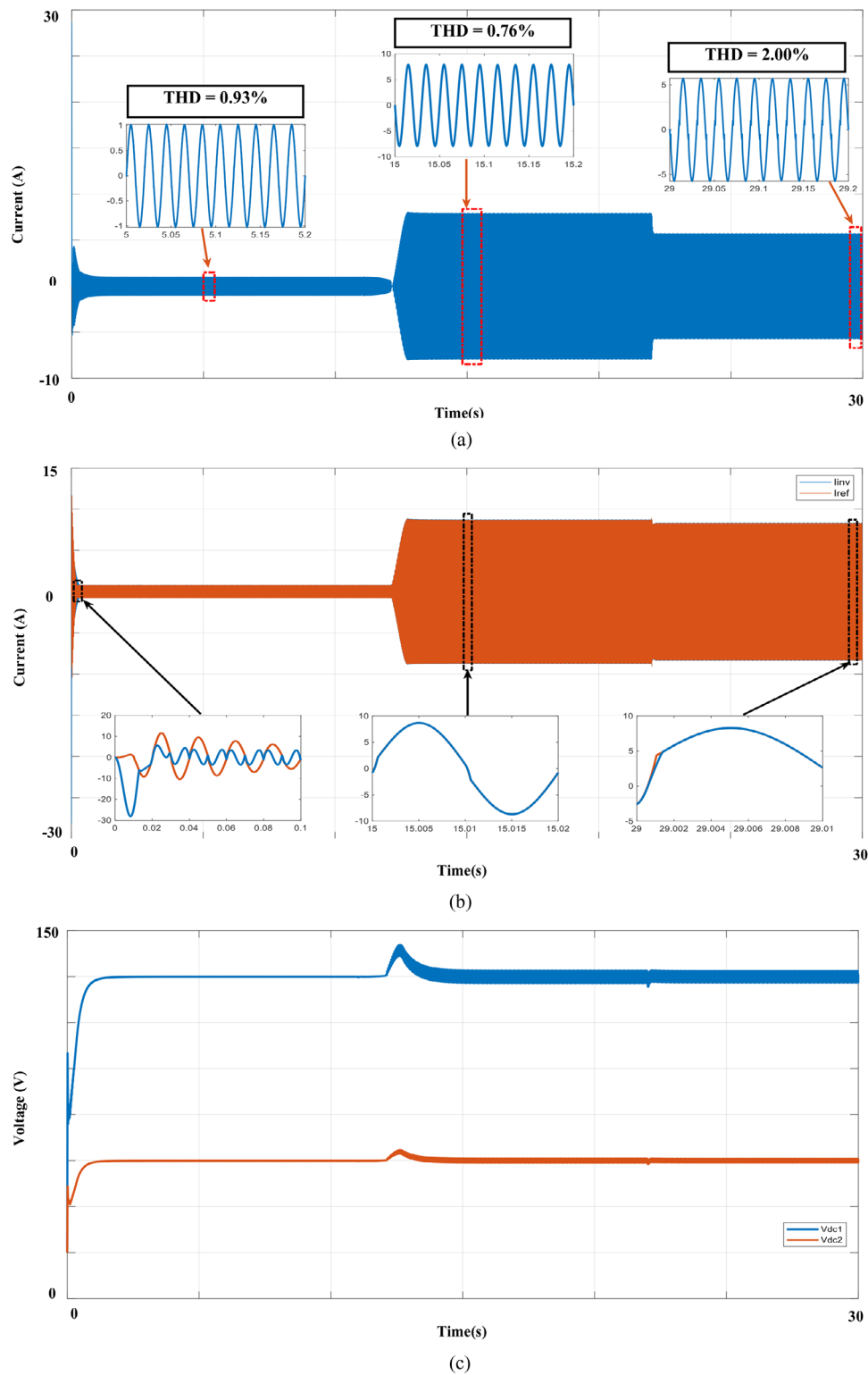


**FIGURE 10** (a) Grid current (b) Inverter current and its reference (c) DC-link capacitor voltages (d) Power of the PV, grid, and load (e) Current of the grid, inverter, and load (f) PV leakage current waveform.

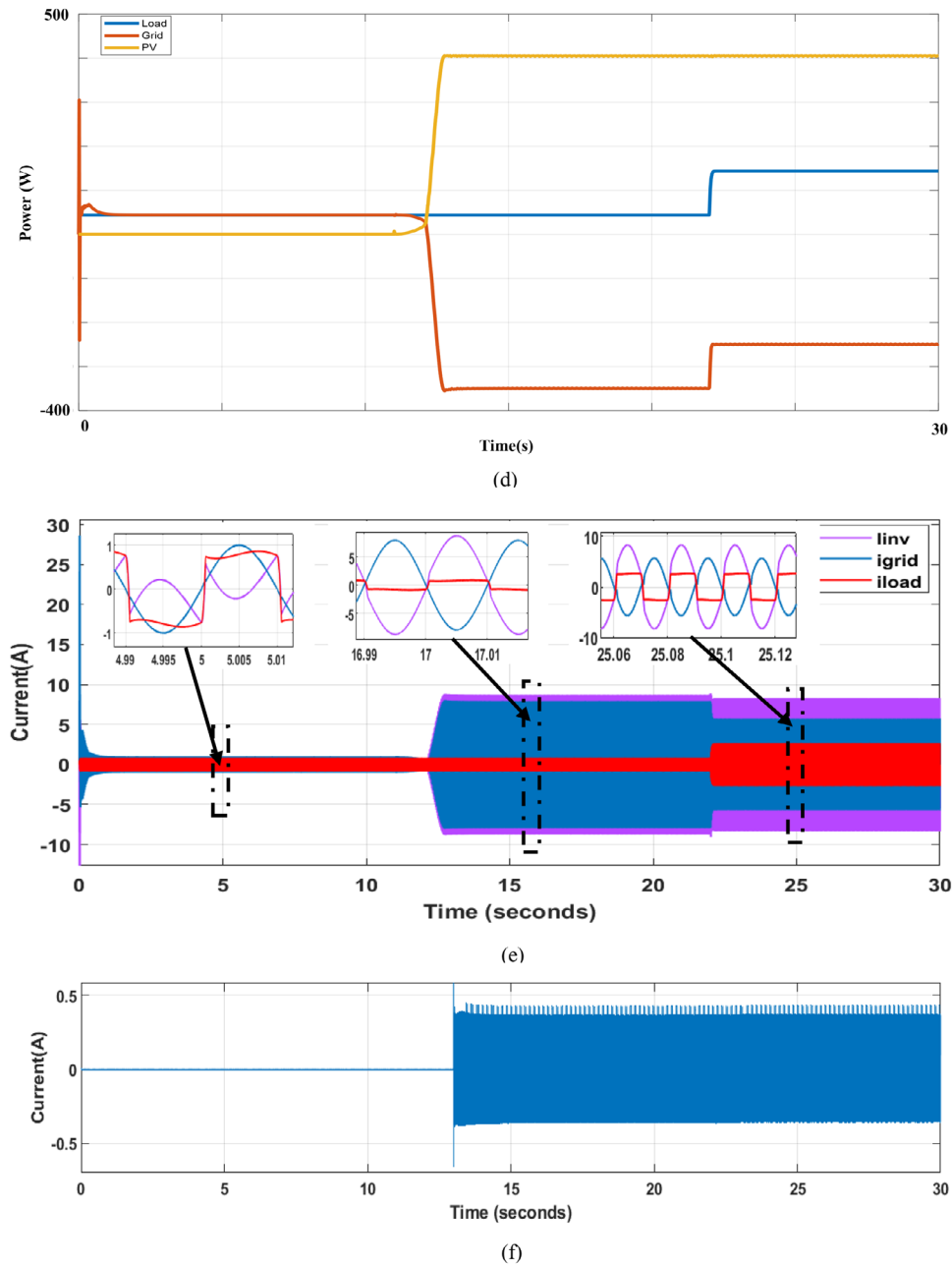


FIGURE 10 Continued

#### 4 | EXPERIMENTAL RESULTS

A laboratory prototype for the proposed multifunction solar active filter has been built using six 600 V, 12A, IGBT active switches of type G4PC30UD. A real-time CU-SLRT Std (DS1104-like interface) is used for the implementation of the different designed controllers (MPPT algorithm, modified p-q controller, and the MPC). The real-time CU-SLRT board offers the same features as those provided by the DS1104 while the computation capabilities are better and more functions are integrated as it includes 6-core 2.6 GHz processor, FPGA-based I/O, 16 analogue inputs, 8 analogue outputs, 16 digital I/O ports, and 16 PWM outputs.

Additionally, it has two encoders and communication interfaces such as Ethernet and RS232 connectors. Figure 11 displays the prototype for the experiment. As the prototype illustrates, the PV array that is composed of 4 PV modules is mounted outdoor the laboratory room. A boost converter connects it to the PUC7 inverter. The real-time CU-SLRT generates pulses to the FPGA card to integrate a 3  $\mu$ s dead time allowing to avoid a short circuit in the PUC7. Finally, the signals are received by the gate drive card to control the six IGBTs of the PUC7 inverter. The most significant advantage of this research is the implementation of grid connected system using an outdoor PV array and without the need of the irradiance and temperature sensors.

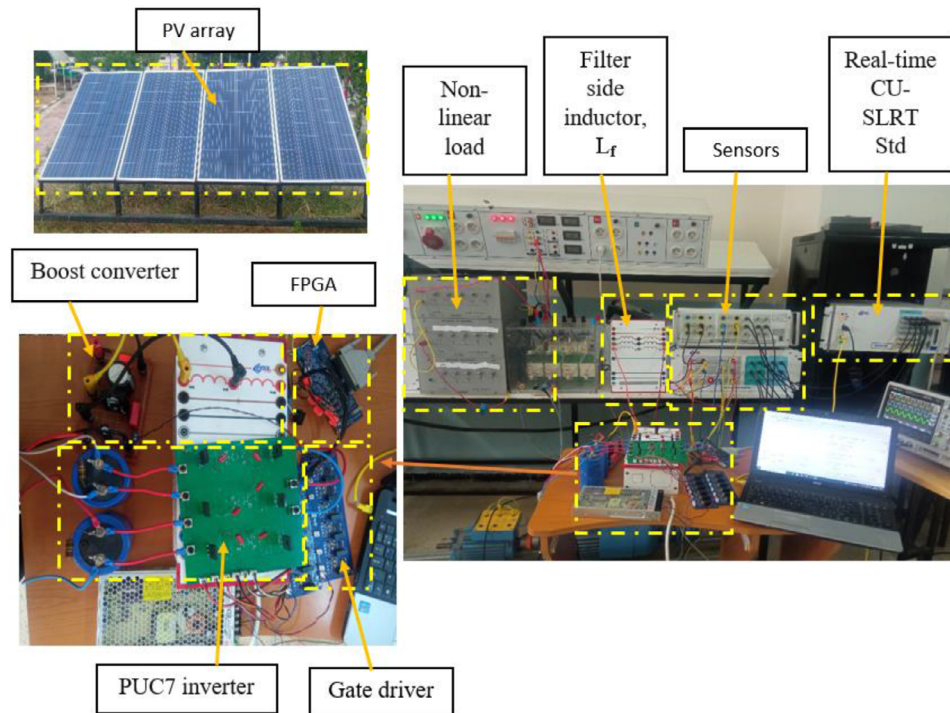


FIGURE 11 The constructed experimental prototype.

Despite the importance of these latter as the validation of the PV array's performance strongly depends on the knowledge of their outputs, however, in this study, the experimental prototype shown in Figure 6 allows to trace the  $I-V$  curve of the PV array at a given moment and subsequently from the maximum power on the  $P-V$  curve is identified ( $V_{mp}$ ,  $P_{mp}$ ). At this time, the experiment shown in Figure 11 is conducted and then the results can be compared with those identified to confirm the suggested control system's efficacy.

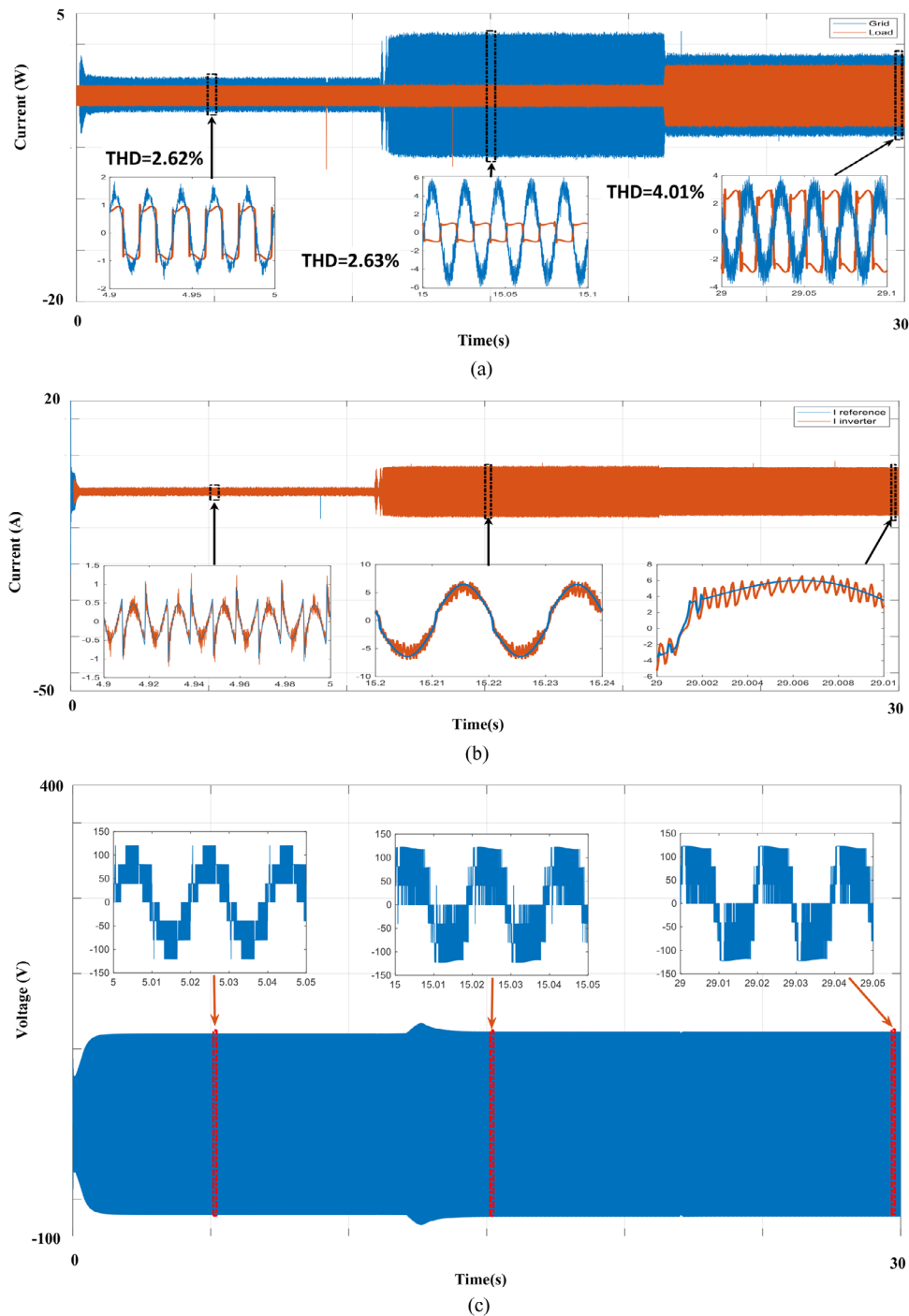
The same system parameters are employed in simulations as they are in practical testing which are shown in Table 3. Furthermore, the sampling frequency of the real-time CU-SLRT is 20 kHz while the controller (MPC) operates at the same frequency. During the experiment, the three scenarios are implemented to facilitate the comparison and highlight the effectiveness of each function of the control system.

Figure 12 presents the empirical findings from our comprehensive experiments, encompassing a diverse set of parameters. These include load and grid currents, inverter output voltage, inverter current, its reference, DC-link capacitor voltages, and power profiles associated with the PV system, grid, and load. Additionally, we delve into grid current and voltage dynamics. In the first scenario ( $t \leq 12$  s), we examine the inverter-generated current (depicted in Figure 12b) to validate the effectiveness of the modified 'p-q' injection method in mitigating harmonics. Notably, the grid current (as shown in Figure 12a) maintains a sinusoidal behaviour, with a THD of 2.62%. During the second scenario ( $t > 12$  s), after connecting the PV array, we observe that the power drawn closely aligns with the maximum power point ( $P_{mp}$ ), as indicated in Figure 8a. Precise computations

reveal an identified  $P_{mp}$  of 403.53 W, while the implemented Perturb and Observe (P&O) algorithm yields  $P_{mp} = 390$  W. Consequently, our MPPT efficiency stands at an impressive 96.65%, comparable to efficiencies reported in prior research [28–31].

Given that the load necessitates approximately 60 W, surplus power remains within the inverter. Our control system intelligently routes this excess power back into the grid utility, as depicted in Figure 12e. Throughout all scenarios, the inverter's output voltage remains remarkably consistent, maintaining the same number of voltage levels (as illustrated in Figure 12c). Furthermore, we demonstrate the efficacy of our proposed MPC by ensuring that the voltage across the second cell capacitor remains constant and equals one-third of the first cell's capacitor voltage (as evidenced by Figure 12d). Lastly, in the third scenario, we vary the resistance of the non-linear load from 70  $\Omega$  to 23  $\Omega$ , resulting in an increased power demand. The effectiveness of our proposed MPC strategy becomes evident through the sustained voltage across the second cell capacitor, consistently maintaining a value equivalent to one-third of the first cell's capacitor voltage (as depicted in Figure 12d). During this scenario, as the non-linear load's resistance varies from 70  $\Omega$  to 23  $\Omega$ , this requires supplying additional power, Figure 12e illustrates an increase in load power to 160 W, accompanied by a corresponding decrease in injected power to 230 W, thus preserving power balance between grid, PV array and load.

As a result, our control system adeptly facilitates power injection into the grid while simultaneously meeting local load requirements and ensuring that THD remains below the IEEE standard threshold. Regarding reactive power compensation, the unity power factor is consistently maintained across all



**FIGURE 12** Experimental results: (a) Load and grid currents, (b) inverter current and its reference, (c) inverter output voltage, (d) DC-link capacitor voltages, (e) power of the PV, grid, and load, (f) grid current and grid voltage (scale V/15), (g) power factor, (h) current of the grid, inverter, and load.

scenarios. During the first scenario, Figure 12g demonstrates a positive unity power factor (with a shift angle of zero), signifying in-phase alignment between grid current and voltage as the grid supplies power to the load (as depicted in Figure 12f). On the other hand, during both the second and third scenarios, where power flows from the PV system to both the grid and the load, Figure 12g illustrates a negative unity power factor (with a shift angle of  $180^\circ$ ), indicating power transfer from the grid to the load.

Furthermore, the good matching between the experimental results and the simulated ones witnesses the accuracy of the proposed control system as well as the identification process.

In Table 4, the comparison between various approaches reveals distinct attributes of each configuration, particularly concerning THD and the simultaneous implementation of the inverter's multifunctionality. The comparison is based on the type of the inverter, the implementation of all functions of the inverter, the value of the THD, and the type of filter. The

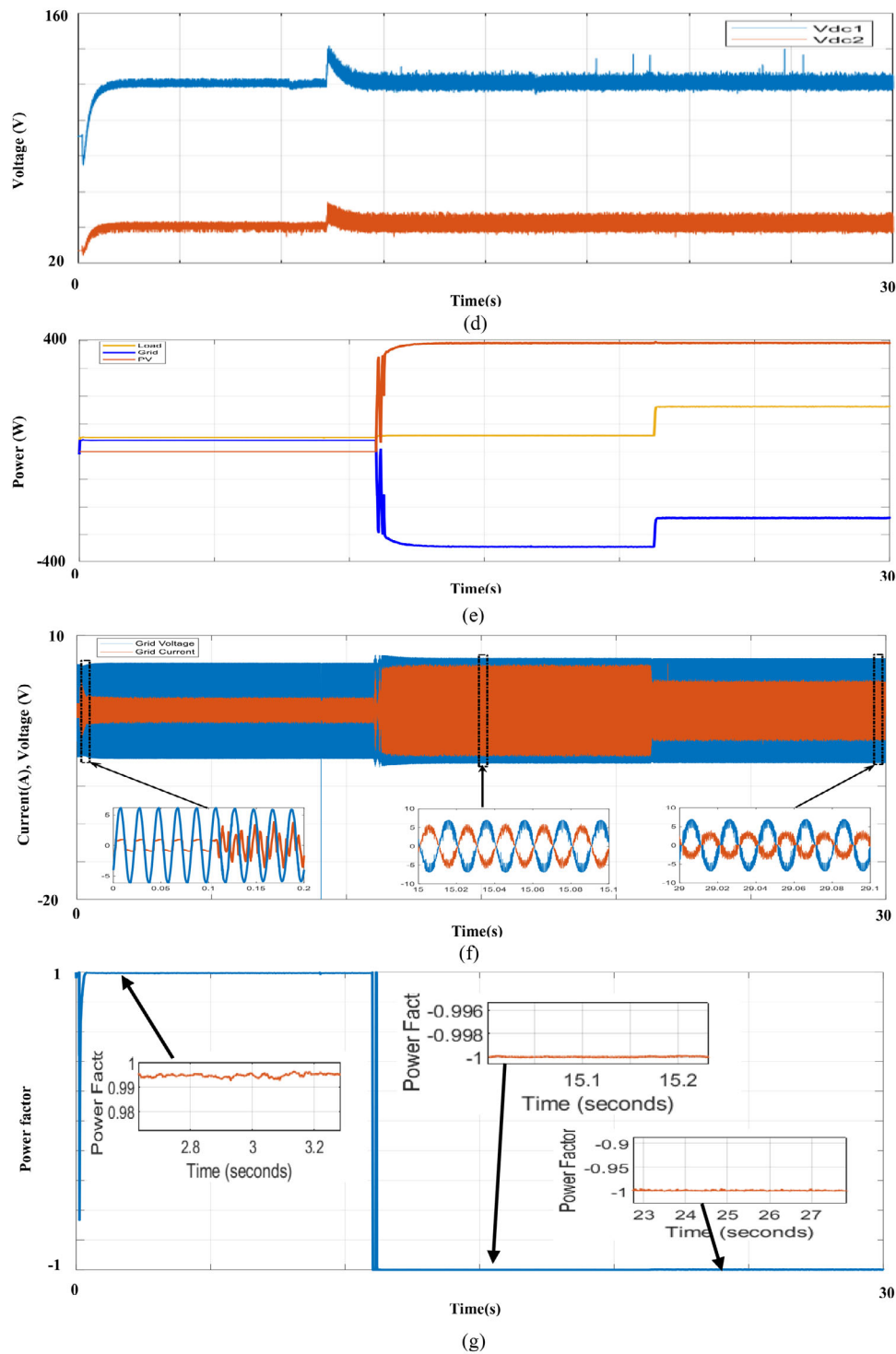


FIGURE 12 Continued

comparison reveals that our approach integrates a multifunctional active power filter for grid power injection, which has been validated using real outdoor conditions.

The absence of irradiance and temperature sensors further distinguishes our approach from both simulation and implementation points of view. With a THD of 2.63% in the grid

current, the proposed configuration showcases the best performance, highlighting its viability for real-world applications. Thus, our proposed configuration stands out for its outdoor validation, multifunctional capabilities, and superior THD performance compared to classical inverters and even PUC5 inverters.

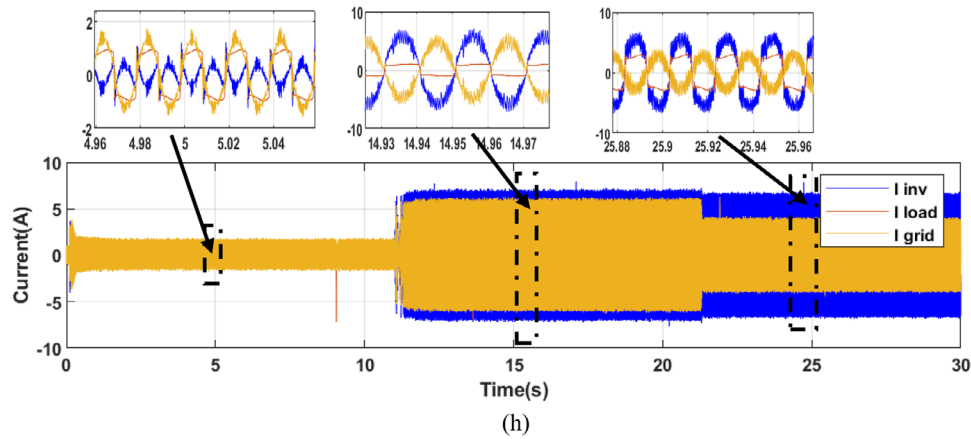


FIGURE 12 Continued

TABLE 4 Comparison with previous work.

Papers	[28]	[29]	[30]	[31]	Proposed configuration
Experimental validation	No	No	Yes	No	Yes
Type of validation	PV simulator	Solar emulator	Real PV indoor validation	HIL	Real PV outdoor validation
APF function	Not included	Included	Included	Included	Included
MPPT	IC	P&O	P&O	VO	P&O
THD of grid current	3.67%	3%	5%	3.11%	2.63%
Filter	LCL	LCL	L	L	L
DC bus controller	PI controller	LQR controller	PI controller	MPC	MPC
Inverter type	H-Bridge Inverter	H-Bridge Inverter	H-Bridge Inverter	MPUC5	PUC7
Test of multifunction simultaneously	No	No	No	Yes	Yes

## 5 | CONCLUSION

In this study, a double-stage, single-phase PUC7 inverter with an MPC control was demonstrated. The inverter is designed to serve multiple purposes, including power injection from the PV array into the grid, reactive power compensation and filtering the grid current harmonics. Various experimental and simulation results were conducted and analysed, which are considered highly relevant and validate the proposed strategies. The system demonstrated good performance across three different scenarios. The proposed  $I-V$  tracer of the PV array allows to effectively check the validity of the MPPT operation. In other words, the identified  $P-V$  curve allows at the moment of the experiment to identify the maximum power point as well as the optimum PV voltage. During the experiment, the extracted maximum power is compared to the identified one to check the performance of the MPPT algorithm. Therefore, conducting outdoor experiments that require the use of sensors is now possible and without the need for these sensors.

Besides, the proposed MPC strategy guarantees stable voltage profiles, even during the variable load conditions. This stability is evidenced by the sustained voltage across capacitors with the required proportionality. A comparative analysis with existing

research highlights the distinction of the proposed approach. Specifically, the operation of multifunctional active power filters under real-life outdoor conditions while THD is minimised and the power factor is unity. Additionally, the P&O algorithm demonstrated its efficiency in tracking and delivering the maximum PV power. As a result, the proposed topology exhibits remarkable flexibility in adapting to load variations, including power factor adjustment, reactive power compensation, and active power injection. The matching observed between our experimental and simulated results serves as compelling evidence for the precision and effectiveness of our control system and identification process and makes the proposed solar active filter configuration a new contribution to the advancement of renewable energy utilization and grid power quality. As a further work, the present study can be extended to verify the MPPT tracking during the variation of the sunlight or irradiance. This can be achieved by finding an automatic way to alter the power output of the PV array. Afterwards, the variation of the PV output can be checked within the same experiment and consequently one may check the MPPT tracking not only under uniform irradiance but also under non-uniform irradiance conditions. Furthermore, the MPC algorithm can be modified as to tolerate the operation of the SAF at reduced sampling frequency



without altering the achieved results in term of THD and power factor.

## AUTHOR CONTRIBUTIONS

**Soufiane Khettab:** Methodology; resources; software; writing—original draft. **Aissa Kheldoun:** Formal analysis; investigation; methodology; resources. **Rafik Bradai:** Conceptualization; data curation; investigation; validation. **Adel Oubelaid:** Investigation; methodology; resources; supervision. **Sandeep Kumar:** Supervision; validation; visualization. **Nima Khosravi:** Investigation; methodology; supervision.

## CONFLICT OF INTEREST STATEMENT

The authors declare no conflicts of interest.

## DATA AVAILABILITY STATEMENT

Data available on request from the authors.

## ORCID

*Nima Khosravi*  <https://orcid.org/0000-0002-2891-1610>

## REFERENCES

- Sarita, K., Saket, R.K., Khan, B.: Reliability, availability, and condition monitoring of inverters of grid-connected solar photovoltaic systems. *IET Renewable Power Gener.* 17(7), 1635–1653 (2023)
- Jogunuri, S., FT, J., Stonier, A.A., Peter, G., Jayaraj, J., Ganji, V.: Random forest machine learning algorithm based seasonal multi-step ahead short-term solar photovoltaic power output forecasting. *IET Renewable Power Gener.* 1–16 (2024)
- Menesy, A.S., Almomin, S., Sultan, H.M., Habiballah, I.O., Gulzar, M.M., Alqahtani, M., Khalid, M.: Techno-economic optimization framework of renewable hybrid photovoltaic/wind turbine/fuel cell energy system using artificial rabbits' algorithm. *IET Renewable Power Gener.* 1–18 (2024)
- Eiva, U.R., Fahim, T.M., Islam, S.S., Ullah, M.A.: Design, performance, and techno-economic analysis of a rooftop grid-tied PV system for a remotely located building. *IET Renewable Power Gener.* 1–17 (2023)
- Khosravi, N., et al.: A novel control approach to improve the stability of hybrid AC/DC microgrids. *Appl. Energy* 344, 121261 (2023)
- Kheldoun, A., Refoufi, L., Khodja, D.E.: Analysis of the self-excited induction generator steady state performance using a new efficient algorithm. *Electr. Power Syst. Res.* 86, 61–67 (2012)
- Bradai, R., Boukenoui, R., Kheldoun, A., Salhi, H., Ghanes, M., Barbot, J.P., Mellit, A.: Experimental assessment of new fast MPPT algorithm for PV systems under non-uniform irradiance conditions. *Appl. Energy* 199, 416–429 (2017)
- Belkhier, Y., et al.: Experimental analysis of passivity-based control theory for permanent magnet synchronous motor drive fed by grid power. *IET Control Theory Appl.* 18(4), 495–510 (2024)
- Chakraborty, S., Mukhopadhyay, S., Biswas, S.K.: A hybrid compensator for unbalanced ac distribution system with renewable power. *IEEE Trans. Ind. Appl.* 59(1), 544–553 (2022)
- Hasan, K., et al.: Shunt active power filter based on Savitzky-Golay filter: Pragmatic modelling and performance validation. *IEEE Trans. Power Electron.* 38, 8838–8850 (2023)
- Wu, T.-F., et al.: PV power injection and active power filtering with amplitude-clamping and amplitude-scaling algorithms. *IEEE Trans. Ind. Appl.* 43(3), 731–741 (2007)
- Pradhan, S., et al.: Performance investigation of multifunctional on-grid hybrid wind–PV system with OASC and MAF-based control. *IEEE Trans. Power Electron.* 34(11), 10808–10822 (2019)
- Kheldoun, A.B.R.B., Bradai, R., Boukenoui, R., Mellit, A.: A new golden section method-based maximum power point tracking algorithm for photovoltaic systems. *Energy Convers. Manage.* 111, 125–136 (2016)
- Khosravi, N., et al.: A new approach to enhance the operation of M-UPQC proportional-integral multiresonant controller based on the optimization methods for a stand-alone AC microgrid. *IEEE Trans. Power Electron.* 38(3), 3765–3774 (2022)
- Defaÿ, F., Llor, A.-M., Fadel, M.: A predictive control with flying capacitor balancing of a multicell active power filter. *IEEE Trans. Ind. Electron.* 55(9), 3212–3220 (2008)
- Junaid, K.M., et al.: Combined T-type and NPC seven-level boost active neutral point clamped inverter for medium voltage applications. *Iran. J. Sci. Technol.* 48(1), 201–212 (2023)
- Tanguturi, J., Keerthipati, S.: Power balancing strategy for cascaded H-bridge inverter in a grid-connected photovoltaic system under asymmetrical operating conditions. *IEEE Trans. Ind. Electron.* 71(6), 5853–5862 (2023)
- Vahedi, H., et al.: Modified seven-level pack U-cell inverter for photovoltaic applications. *IEEE J. Emerging Sel. Top. Power Electron.* 6(3), 1508–1516 (2018)
- Khawaja, R., Sebaaly, F., Kanaan, H.Y.: Design of a 7-level single-stage/phase PUC grid-connected PV inverter with FS-MPC control. In: 2020 IEEE International Conference on Industrial Technology (ICIT). Buenos Aires, Argentina (2020)
- Chebbah, M.T., Vahedi, H., Al-Haddad, K.: Real-time simulation of 7-level Packed U-Cell shunt active power filter. In: 2015 IEEE 24th International Symposium on Industrial Electronics (ISIE). Buzios, Brazil (2015)
- Vahedi, H., Al-Haddad, K.: Real-time implementation of a seven-level packed U-cell inverter with a low-switching-frequency voltage regulator. *IEEE Trans. Power Electron.* 31(8), 5967–5973 (2015)
- Vahedi, H., Labbé, P.-A., Al-Haddad, K.: Sensor-less five-level packed U-cell (PUC5) inverter operating in stand-alone and grid-connected modes. *IEEE Trans. Ind. Inf.* 12(1), 361–370 (2015)
- Metri, J.L., et al.: Real-time implementation of model-predictive control on seven-level packed U-cell inverter. *IEEE Trans. Ind. Electron.* 63(7), 4180–4186 (2016)
- Dekka, A., et al.: Model predictive control of high-power modular multilevel converters—An overview. *IEEE J. Emerging Sel. Top. Power Electron.* 7(1), 168–183 (2018)
- Pourmirasghariyan, M., et al.: A maximum power point tracking scheme for PV systems using model predictive control in grid-connected packed U-cell inverters. In: 2022 12th Smart Grid Conference (SGC). Kerman, Iran, Islamic Republic of (2022)
- Rodriguez, J., Cortes, P.: *Predictive Control of Power Converters and Electrical Drives*. John Wiley & Sons, Hoboken, NJ (2012)
- Maldonado, J.L., et al.: Optimal planning of collective photovoltaic arrays in energy communities through a multi-cut benders' decomposition strategy. *Sustainable Cities Soc.* 104, 105307 (2024)
- Sun, Y., et al.: Artificial neural network for control and grid integration of residential solar photovoltaic systems. *IEEE Trans. Sustainable Energy* 8(4), 1484–1495 (2017)
- Arab, N., et al.: A multifunctional single-phase grid-integrated residential solar PV systems based on LQR control. *IEEE Trans. Ind. Appl.* 55(2), 2099–2109 (2018)
- Wu, T.-F., et al.: A single-phase inverter system for PV power injection and active power filtering with nonlinear inductor consideration. *IEEE Trans. Ind. Appl.* 41(4), 1075–1083 (2005)
- Oubelaid, A., et al.: Health-conscious energy management strategy for battery/fuel cell electric vehicles considering power sources dynamics. *J. Energy Storage* 68, 107676 (2023)
- Sahli, A., et al.: Energy management and power quality enhancement in grid-tied single-phase PV system using modified PUC converter. *IET Renewable Power Gener.* 13(14), 2512–2521 (2019)
- Belmadani, H., et al.: A twofold hunting trip African vultures algorithm for the optimal extraction of photovoltaic generator model parameters. *Energy Sources Part A* 44(3), 7001–7030 (2022)
- Vazquez, S., et al.: Model predictive control for power converters and drives: Advances and trends. *IEEE Trans. Ind. Electron.* 64(2), 935–947 (2016)

35. Kheldoun, A., et al.: A new golden section method-based maximum power point tracking algorithm for photovoltaic systems. *Energy Convers. Manage.* 111, 125–136 (2016)
36. Mohapatra, A., et al.: A review on MPPT techniques of PV system under partial shading condition. *Renewable Sustainable Energy Rev.* 80, 854–867 (2017)
37. Al-Haddad, K., Ounejjar, Y., Gregoire, L.-A.: Multilevel electric power converter. US Patent 9,331,599 B2 (2011)
38. Akagi, H., Kanazawa, Y., Nabae, A.: Instantaneous reactive power compensators comprising switching devices without energy storage components. *IEEE Trans. Ind. Appl.* IA-20(3), 625–630 (1984)
39. Khadkikar, V., Chandra, A., Singh, B.N.J.I.P.E.: Generalised single-phase pq theory for active power filtering: Simulation and DSP-based experimental investigation. *IET Power Electron.* 2(1), 67–78 (2009)
40. Sahli, A., Krim, F., Laib, A., Talbi, B.: Energy management and power quality enhancement in grid-tied single-phase PV system using modified PUC converter. *IET Renewable Power Gener.* 13(14), 2512–2521 (2019)
41. Tlenshiyeva, A., et al.: A data-driven methodology to design user-friendly tariffs in energy communities. *Electric Power Syst. Res.* 228, 110108 (2024)

**How to cite this article:** Khettab, S., Kheldoun, A., Bradai, R., Oubelaid, A., Kumar, S., Khosravi, N.: Performance evaluation of PUC7-based multifunction single-phase solar active filter in real outdoor environments: Experimental insights. *IET Renew. Power Gener.* 18, 1740–1757 (2024).  
<https://doi.org/10.1049/rpg2.13028>